

## QCD Tests in High Energy Collisions<sup>a</sup>

I. Bertram<sup>1</sup>, T. Carli<sup>2</sup>, G. Gustafson<sup>3</sup>, J. Hartmann<sup>4</sup>

*1) Northwestern University, USA*

*2) Max-Planck Institut München, Germany*

*3) Lund University, Sweden*

*4) McGill Institute, Montréal, Canada*

Recent measurements and theoretical developments on the hadronic final state in deep-inelastic scattering,  $p\bar{p}$  and  $e^+e^-$  collisions are presented.

### 1 Introduction

The hadronic final state in high energy collisions provides a testing ground for the strong interaction and its underlying theory QCD. The large center of mass energy ( $\sqrt{s} \approx 300\text{GeV}$ ) available at the  $e^\pm p$  collider HERA allows the production of hadrons in deep-inelastic scattering (DIS) to be explored in a new kinematic regime. A wide range of the squared momentum transfer  $Q^2$  from  $Q^2 \approx 0 - 10^5 \text{ GeV}^2$  can be accessed. At the same time very low values of the Bjorken scaling variable  $x_{Bj}$  down to  $10^{-5}$  can be reached.

The large data samples do not only allow to study hard processes, but also focus the interest of experimentalists and theorists on details of the complex parton dynamics and the hadronisation of partons to observable hadrons. Recently, much effort has been put into the calculation of next-to-leading order (NLO) effects, on a consistent incorporation of the parton evolution into flexible Monte Carlo programs and approaches to study power suppressed hadronisation corrections for specific variables.

Results from the  $p\bar{p}$  collider TEVATRON operating at a center of mass energy  $\sqrt{s} = 630 \text{ GeV}$  and  $1.8 \text{ TeV}$  and of the  $e^+e^-$  colliders LEP I  $\sqrt{s} = 91 \text{ GeV}$  and LEP II  $130 < \sqrt{s} \lesssim 190 \text{ GeV}$  overlap in many kinematic ranges and provide complementary information. While at the TEVATRON one has access to very high  $E_T$  phenomena allowing to probe very short distances, LEP provides a clean environment to examine QCD effects. The different center of mass energies from  $3$  to  $190 \text{ GeV}$  available in  $e^+e^-$  experiments, allow the evolution of QCD phenomena to be investigated<sup>3</sup>. The unique advantage of HERA is that one can probe QCD at different scales in one experiment. Varying experimental conditions can be realized only by controlling the scattered electron.

Detailed comparison of hadron production in different reactions can be performed and universality of perturbative QCD (pQCD) can be tested.

---

<sup>a</sup>Summary of Working Group III 'Hadronic Final State', 6th International Workshop on Deep Inelastic Scattering and QCD, Brussels (Belgium), 04-08 April 1998.

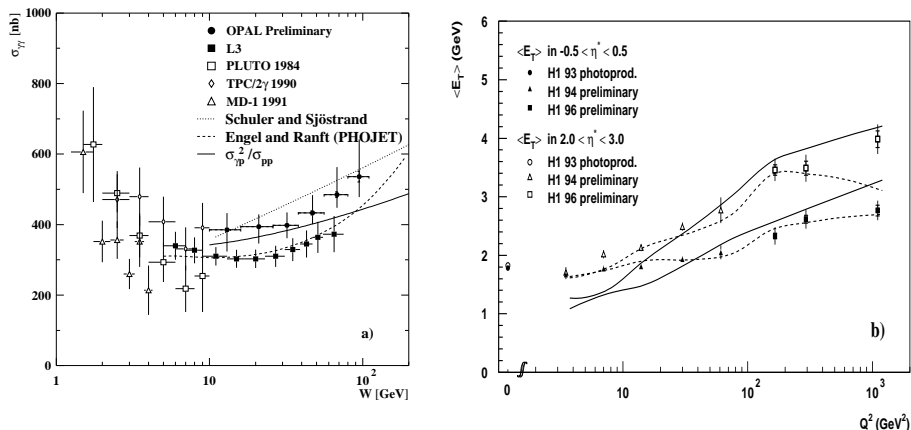


Figure 1: a) Total cross-section  $\sigma_{\gamma\gamma} \rightarrow \text{hadrons}$  as a function of the invariant mass of the hadronic final state  $W$ . b)  $\langle E_T \rangle$  in two rapidity regions in the hCMS as a function of  $Q^2$ . Overlaid are the Monte Carlo predictions from LEPTO (solid) and CDM (dashed).

## 2 Photons in High Energy Collisions

In the quark parton model a highly virtual photon interacts with a parton freely moving in the proton. This is a good approximation when small distances are probed, i.e. in the limit where  $Q^2$  is large. In this regime, the photon behaves like a point-like object, i.e. it directly couples to quarks to produce the hard scattering. At low virtualities the photon dominantly fluctuates into vector mesons. The photon may also fluctuate into a  $q\bar{q}$  state with higher transverse energy without forming a bound state. In this case the photon acts as a source of strongly interacting partons. Such a process can be calculated within pQCD using the concept of a photon structure function.

Photon-photon interactions at high center of mass energies can be studied at LEP I and LEP II using doubly anti-tagged  $e^+e^-$  scattering events. They provide the main source of hadron production above the  $Z^0$  mass. The total cross section  $\sigma_{\gamma\gamma} \rightarrow \text{hadrons}$  is measured by L3 and OPAL <sup>4</sup> (see Fig. 1a). The LEP II data together with earlier results <sup>5</sup> at small energies show the characteristic slow rise expected from the hadronic nature of the photon for increasing invariant masses  $W$  of the hadronic final state in the event. Such a rise is consistent with the universal behaviour of the total cross-section <sup>6</sup> in  $\gamma p$  scattering at HERA <sup>7</sup> and in  $p\bar{p}$  collisions at TEVATRON <sup>8</sup>. It is well described by QCD models <sup>9</sup>. The two recent measurements show a similar  $W$  dependence, but disagree in the absolute values (see Fig. 1a).

Events where the perturbatively calculable components become more im-

portant can be selected by tagging heavy quarks in the final state. The cross-section  $e^+e^- \rightarrow e^+e^-c\bar{c}$  measured<sup>10</sup> as a function of  $\sqrt{s}$  is well described by a full NLO calculation<sup>11</sup>. A substantial resolved contribution is required.

In DIS, the hadronic nature of the photon can be illustrated in the reference frame where the proton is at rest and the photon is fast. In this frame the photon fluctuates - before interacting with the proton - into a complex object with a typical size of  $c\tau_\gamma = 200$  fm at  $x_{Bj} \approx 10^{-3}$ . For suitable observables one can find characteristic properties of hadron-hadron collisions in DIS at low- $x_{Bj}$ . When comparing the  $\langle E_T \rangle$  produced in the central pseudo-rapidity bin  $|\eta| < 0.5$  of the hadronic center of mass system (hCMS) to hadron-hadron collisions, it scales with the available center of mass energy ( $\sqrt{s}$  or  $W$ ) independent of the nature of the incoming particle<sup>12</sup>. In an early publication<sup>13</sup>, the H1 collaboration has shown that at fixed  $W = 180$  GeV the  $\langle E_T \rangle$  in  $|\eta| < 0.5$  is independent of the photon virtuality. At this conference, new results in an extended kinematic range and with a better understanding of systematics effects have been presented<sup>14</sup>. The  $\langle E_T \rangle$  in the central bin is constant for  $0 \lesssim Q^2 \lesssim 50$  GeV<sup>2</sup>, but then rises (see Fig. 1b). Since the typical short range correlation in inelastic hadron-hadron collisions is about  $\Delta\eta \lesssim 2$ , the  $E_T$  induced by the photon virtuality should become negligible in this region. The unexpected rise might be associated with a kinematic shift of the highest  $E_T$  position as a function of  $Q^2$  (see Fig. 3 in ref.<sup>14</sup>). It would be interesting to see, if after a redefinition of the fragmentation and central rapidity bin, the expected constant behaviour of the  $\langle E_T \rangle$  can be verified in the data.

### 3 Heavy Quarks in (real) Photon-Proton Collisions

At HERA, heavy quarks are dominantly produced in real  $\gamma$ -p collisions. They can be identified via tagging hadrons forming bound states of heavy quarks alone (hidden) or heavy and light quarks (open).

Recent NLO calculation for charm production apply two schemes. In the massive scheme<sup>15</sup> the charm mass provides a natural hard scale and charm quarks only appear in the hard subprocess, this means that they are not an active flavour in the parton evolution. In the massless scheme<sup>16</sup> charm is treated like any other light quark. Terms proportional to  $\alpha_s \ln(p_t^2/m_c^2)$  in the parton evolution are summed to all orders, but charm mass effects are ignored. This approach should give a better description of data, if  $p_t^2/m_c^2$  is large. To compute the  $D^*$  cross-section one needs an appropriate fragmentation function, like the Peterson function<sup>17</sup>, which is constrained by  $e^+e^-$ -data. Another approach is to complement a LO matrix element by higher order contributions based on the BFKL evolution of an unintegrated gluon distribution<sup>18</sup>.

The differential cross-section  $d\sigma/dp_t$  for  $|\eta| < 1.5$  and  $d\sigma/d\eta$  for  $p_t >$

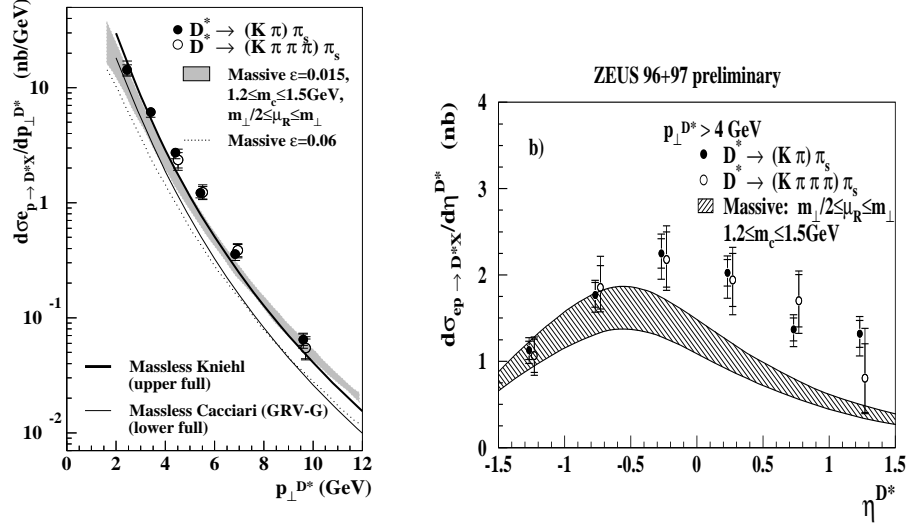


Figure 2:  $D^*$  cross-section versus a) the trans. momentum and b) the pseudorapidity.

4 GeV measured for two  $D^*$  decay channels<sup>19</sup> is shown in Fig. 2. None of the NLO approaches is able to describe the data. The discrepancy is most pronounced in the direction towards the proton remnant. This is, however, the region where the variation of theory parameters like the gluon density in the photon, the charm mass, the renormalisation scale or the fragmentation parameters (e.g.  $\varepsilon$ ) have the smallest influence. To get more information on event kinematics a subsample containing hard dijets with  $E_{T,1} > 6$  and  $E_{T,2} > 7$  GeV and  $|\eta^{jet}| < 2.4$  is selected. A comparison of  $d\sigma_{dijet}/dx_{\gamma}^{OBS}$  to a LO QCD model shows a significant contribution from resolved events (in a LO interpretation) at low  $x_{\gamma}^{OBS} < 0.75$ . In contrast to the inclusive dijets analysis, a LO QCD model is able to describe the absolute cross-section. A massive NLO calculation fails at low  $x_{\gamma}^{OBS}$  to describe the data. It will be interesting to compare the data also to a massless scheme which should give a better description at high  $p_t$ .

Open  $b$  production has been studied for the first time at HERA using the semi-leptonic decay channels. Dijet events accompanied by at least one muon within one jet in the final state are selected. The probability that (misidentified) muons originate from other hadrons like pions, kaons or protons is extracted from the data and cross-checked by a detector simulation. The content of fake muon in the data sample is about 24%. The beauty and charm contribution is

deduced on a statistical basis exploiting that the  $p_t$  of the muon relative to the jet thrust axis is higher for  $b$  events. A relative fraction of  $\approx 52\%$  for beauty and  $24\%$  for charm is found. The measured visible cross-section for  $0.1 < y < 0.8$ ,  $p_t^\mu > 2$  GeV and  $35 < \theta^\mu < 130^\circ$  is  $0.93 \pm 0.08(\text{stat.})^{+0.21}_{-0.12}(\text{syst.})$  nb. This cross-section is about 5 times larger than the LO QCD model AROMA<sup>20</sup> prediction. NLO calculations<sup>21</sup> are not yet available for the specific analysis cuts. However, corrections not higher than a factor of 2 are expected. The unexpected high  $b$  cross-section might explain part of the  $D^*$  excess in the forward region.  $b$  events are produced more forward (see Fig. 2b in ref.<sup>22</sup>) and the  $D^*$  appears in a large fraction of the  $b$  decay channels.

#### 4 Jet Shapes

The internal structure of jets provides useful information on the transition of a parton to the complex aggregate of observable hadrons. Since jets are used as manifestations of hard partons in many studies of pQCD, it is important to prove that their detailed properties can be well described.

The (differential) jet shape  $\Psi(r)$  ( $\rho(r)$ ) is defined as the average fraction of the  $E_T$  of the jets inside an inner cone of radius  $r$  (inside a cone slice with width  $\Delta r_0$ ) concentric to the outer jet cone with radius  $R = 1$ :

$$\Psi(r) = \frac{1}{N_{\text{jet}}} \sum_{\text{jets}} \frac{E_T(0, r)}{E_T(0, R)}, \quad \rho(r) = \frac{1}{N_{\text{jet}}} \sum_{\text{jets}} \frac{E_T(r - \Delta r_0/2, r + \Delta r_0/2)}{\Delta r_0 E_T(0, R)}, \quad (1)$$

where  $N_{\text{jet}}$  is the number of jets. By definition  $0 < \Psi < 1$  and  $\Psi(R) = 1$ . The steepness of the rise (fall) of  $\Psi$  ( $\rho$ ) describes the collimation of the jet.

Jet shapes corrected for detector effects have been measured by ZEUS<sup>23,24</sup> for DIS at  $Q^2 > 100$  GeV<sup>2</sup> in the laboratory frame using jets with  $E_{T,\text{lab}} > 14$  GeV and  $-1 < \eta_{\text{lab}} < 2$ . The differential jet shape peaks around 0 and falls down by a factor of 40 towards the edge of the jet (see Fig. 3). Jets become narrower as  $E_T$  increases. No  $\eta$  dependence is found. Jets produced in neutral and charged current interactions as well as in  $e^+e^-$  interactions<sup>25</sup> behave in a similar way.

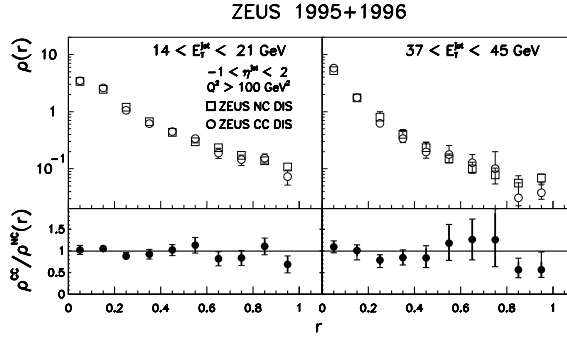


Figure 3: Jet shapes in neutral current and charged current events in two different  $E_T$  bins in the lab. frame for  $Q^2 > 100$  GeV<sup>2</sup>.

The H1 analysis<sup>26</sup> is performed at  $10 < Q^2 < 120 \text{ GeV}^2$ . Jets with  $E_T > 5 \text{ GeV}$  and  $-1 < \eta_{\text{lab}} < 2$  are selected in a dijet sample in the Breit frame.

In the phase space region chosen by H1, jets get less collimated towards the proton remnant direction. Another interesting observable is the mean number of subjets defined by a repetition of the clustering procedure<sup>b</sup> within a selected jet. The clustering is stopped when all particles are above some cut-off  $y_{\text{cut}}$ . Remaining particles are called subjets. As is shown in Fig. 4 the number of subjets decreases for higher  $E_T$  (for  $\eta > 2.2$ ) and in particular for low  $E_T$  more subjets are found towards the target region.

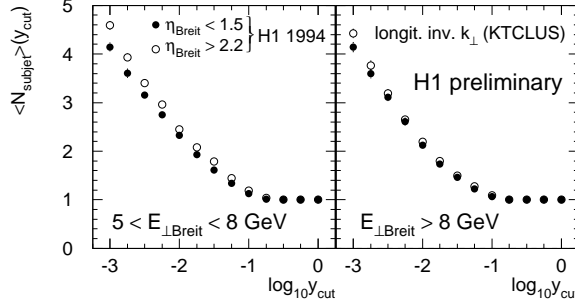


Figure 4: Mean subjet multiplicity for dijets at low  $Q^2$  with  $E_T > 5 \text{ GeV}$  as a function  $y_{\text{cut}}$ .

Remaining particles are called subjets. As is shown in Fig. 4 the number of subjets decreases for higher  $E_T$  (for  $\eta > 2.2$ ) and in particular for low  $E_T$  more subjets are found towards the target region.

## 5 Jet Production in Real Photon-Proton Collisions

Hard jets allow precise tests of basic QCD predictions. The largest event samples of high  $E_T$  jets at HERA are available in (real) photon proton collisions. Many subprocesses with different angular distributions contribute to the total dijet cross-section. In the resolved channel gluon exchange dominates and leads to a  $(1 - |\cos \vartheta^*|)^{-2}$  distribution<sup>c</sup>. For events where the photon couples directly, a quark is dominantly exchanged. The angular distribution is then of the form  $(1 - |\cos \vartheta^*|)^{-1}$ . Events from resolved processes are therefore in LO  $\alpha_s$  expected to rise more steeply towards small  $\vartheta^*$  and the relative contribution of direct to resolved processes should increase with increasing jet  $E_T$  (since  $\cos \vartheta^* = 1 - 4 E_T^2/s$ ).

Resolved and direct processes can be operationally defined by a cut on  $x_\gamma^{\text{OBS}}$  defined by  $\sum_{jet}(E - P_z)/\sum_{had.}(E - P_z)$ . In LO,  $x_\gamma^{\text{OBS}}$  can be interpreted as the fraction of the longitudinal momentum carried by the interacting parton in the photon. It should be 1 for direct and smaller for resolved processes. In NLO the direct and resolved components of the total cross-section are strongly correlated. The operational definition ( $x_\gamma^{\text{OBS}} < 0.75$ ) performed in the experimental analysis to enhance the resolved component

<sup>b</sup>Jets are here defined by the longitudinal invariant  $k_t$  algorithm for DIS<sup>27</sup>.

<sup>c</sup> $\vartheta^*$  is the angle between the jet with the highest  $E_T$  and the beam direction in the center-of-mass system of the hard subprocess.

leads to a sizeable mixture between NLO point-like and resolved components.

In Fig. 5 the angular distribution for dijet events produced in  $e^\pm p$ <sup>28</sup> and  $e^+e^-$  collisions<sup>4</sup> are shown<sup>d</sup>. The qualitative behaviour known from LO arguments is seen in the data. It has been, however, pointed out<sup>29</sup> that in a NLO calculation the characteristic  $1 - |\cos \vartheta^*|$  distribution is not a result of the different propagator in resolved and direct processes (both distributions are flat), but are generated

by the kinematical cuts  $M_{jj} > 23$  GeV and  $|\eta| < 0.5$  applied in the  $e^\pm p$  analysis<sup>e</sup>. The steeper rise for low  $x_\gamma^{\text{OBS}}$  is induced by a softer  $M_{jj}$  distribution. It is therefore not clear, if an operational definition is useful to extract information on the underlying dynamics.

Properties of events with three jets can be compared to  $\mathcal{O}(\alpha_s^2)$  QCD calculations<sup>30,31</sup> which represent the LO for such processes. A basic quantity is the invariant mass of the three jet system  $M_{3j}$ . The  $M_{3j}$  distribution<sup>32</sup> shown in Fig. 6 is reasonably well described by  $\mathcal{O}(\alpha_s^2)$  calculations. The LO QCD models like PYTHIA<sup>33</sup> or HERWIG<sup>34</sup> fail in absolute, but are able to reproduce the shape. In three jet events, in addition to the polar angle  $\cos \vartheta_3$  of the jet with the highest  $E_T$  and the beam direction,  $\Psi$ , the angle between the plane containing the three jets and the plane containing the highest  $E_T$  jet and the beam direction, can be defined. The measured  $\cos \vartheta_3$  is different from what is expected from pure phase space arguments (see Fig. 6b).  $\mathcal{O}(\alpha_s^2)$  QCD calculations and the LO QCD models give a good description of the data. Due to the selection cuts the phase space near  $\Psi \approx 0$  and  $\Psi \approx \pi$  is artificially suppressed. Nevertheless, a strong tendency for the three jet plane to lie near the plane containing the beam and the highest  $E_T$  jet can be seen in the data. Such a characteristic behaviour is expected from the collinear singularities of QCD radiation.

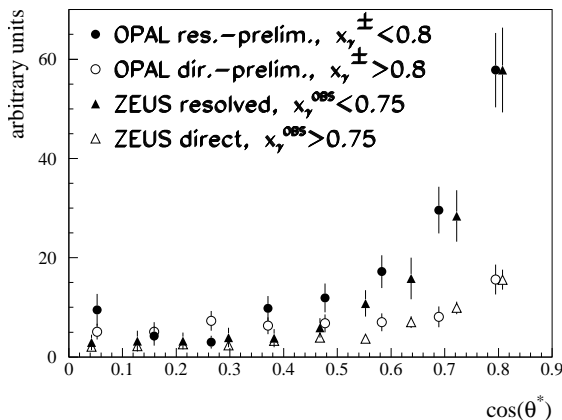


Figure 5: Distribution of the polar angle of the highest  $E_T$  jet with respect to the beam in the rest frame of the 2 jet system.

<sup>d</sup>In the case of  $e^+e^-$ :  $x_\gamma^\pm = \sum_{\text{jet}} (E \pm P_z) / \sum_{\text{had.}} (E \pm P_z) < 0.8$  is used.

<sup>e</sup>Similar cuts have been applied in the  $e^+e^-$  analysis:  $M_{jj} > 12$  GeV and  $|\eta| < 2$ .

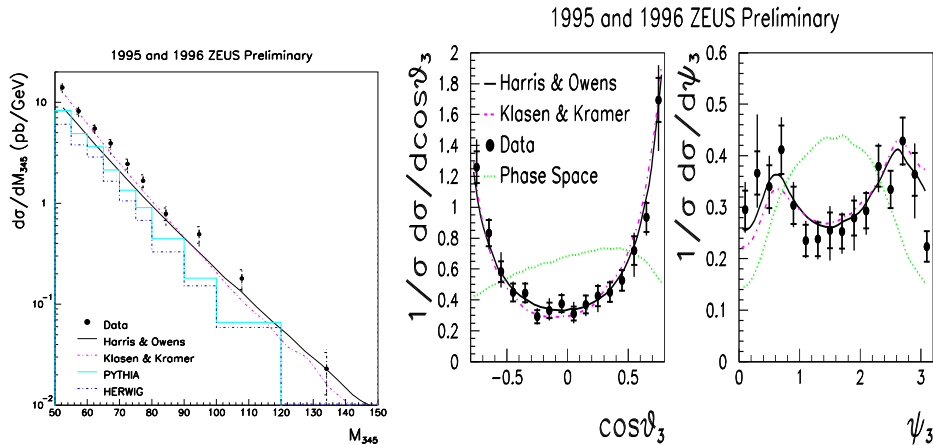


Figure 6: a) Invariant mass of the 3-jet system. b) Angular distributions for jets with respect to certain planes of the event, see text for details.

## 6 Jet Production in DIS

The production rate of dijet events in DIS is directly sensitive to the QCD free parameters like the strong coupling constant  $\alpha_s$  or the parton density functions in the proton. The possibility to perform NLO precision tests has stimulated a lot of activity since the beginning of HERA<sup>35,36,37</sup>. Early analyses were restricted to semi-analytical NLO calculations<sup>38,39</sup> which were only available for the JADE algorithm<sup>40</sup>. These calculations did, however, not use exactly the same jet definitions as in the experimental analysis<sup>41</sup>. Moreover, approximations were made which turned out not to be valid over the full phase space region<sup>42</sup>. Meanwhile the flexible NLO Monte Carlo programs MEPJET<sup>42</sup>, DISENT<sup>43</sup>, DISASTER++<sup>45</sup> and JETVIP<sup>44</sup> became available which allow arbitrary jet definition schemes and experimental cuts. The H1 collaboration has now updated their results<sup>f</sup> on the  $\alpha_s$  determination from integrated and differential jet rates<sup>47</sup> using the JADE algorithm.

At the DIS 97 conference, agreement of NLO calculations with the data could only be achieved in very restricted phase space regions<sup>48</sup>. Especially in the region of low  $Q^2$ , both NLO calculations and LO QCD models failed to describe the data. This had been interpreted as a sign of a contribution of (LO) resolved photons in DIS<sup>49</sup>, but it was not clear why the shape of all distributions associated to the hard subprocess were well described by NLO calculations.

<sup>f</sup>The ZEUS results do not change when using the new NLO calculations<sup>46</sup>.



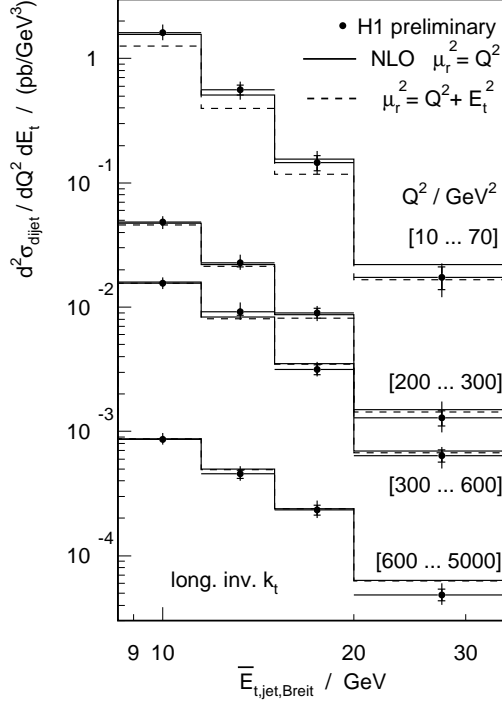


Figure 7: Double differential dijet cross-section in the Breit system NLO calculations with different choices of the renormalisation scales are overlayed.

$5 < Q^2 < 100 \text{ GeV}^2$ , where  $\Delta > 2$  or  $E_{T,1} + E_{T,2} > 13 \text{ GeV}$  is required, are well described by NLO calculations.

The H1 collaboration has presented a comprehensive measurement<sup>26</sup> of the double differential dijet cross-section corrected for detector effects from  $10 < Q^2 < 5000 \text{ GeV}^2$  and  $8.5 < \langle E_T \rangle \lesssim 35 \text{ GeV}$ . Jets defined in the Breit frame with several jet algorithms<sup>27,52,53</sup> are required to have  $E_T > 5 \text{ GeV}$  and  $E_{T,1} + E_{T,2} > 17 \text{ GeV}$ . The interplay between the two hard scales  $Q^2$  and  $E_T$  can be seen in the data (see Fig. 7). The  $\langle E_T \rangle$  spectra of the jets get harder for increasing  $Q^2$ . A NLO calculation<sup>43</sup> provides a good description over the whole kinematic range<sup>9</sup>. These are the first encouraging steps towards a fundamental understanding of dijet production in DIS at HERA. At low  $Q^2$  NLO corrections are large. Moreover, they depend on the choice of the

Meanwhile, it has been understood that this discrepancy only occurs when both jets are required to be above the same  $E_T$  threshold. As  $\Delta$ , the required  $E_T$  difference of the jet thresholds, approaches 0, a fixed order calculation gets infra-red sensitive<sup>29</sup>. In events where the  $E_T$  of the jets are approximately equal, no phase space to emit a third real parton is available. This leads to an incomplete cancellation between real and virtual corrections at the threshold and makes a fixed order calculation unpredictable<sup>29,50</sup>. A resummation of higher orders is necessary at this phase space point. First theoretical attempts for resummation of dijet production in hadron hadron collisions have been presented at this conference<sup>51</sup>.

The updated dijet rates<sup>26</sup> for

<sup>9</sup> Hadronisation corrections are below 7% for  $Q^2 > 200 \text{ GeV}^2$  and below 15% for lower  $Q^2$ .

renormalisation scale. A good description of the data can only be achieved using  $Q^2$  as scale. The conceptually preferred scale  $Q^2 + E_T^2$  providing a natural interpolation between the Bjorken and the photoproduction limit falls below the data. It is an open question whether the success of the  $Q^2$  scale is accidental and whether the failure of the  $Q^2 + E_T^2$  scale is a sign that higher orders can give significant contributions at low  $Q^2$ .

The question to which extent contributions from resolved photons are needed to describe the data can be addressed using the NLO program JETVIP<sup>44</sup> incorporating the NLO Matrix elements together with a virtual photon structure function. Higher order emissions in the photon direction beyond the one which is already included in the NLO matrix elements (mainly the diagram where the photon splits into a  $q\bar{q}$  pair) are only needed in the region of low  $Q^2$ .

## 7 DGLAP / BFKL Parton Evolution Dynamics

Several talks concentrated on the parton evolution dynamics at low  $x_{Bj}$ <sup>54,55,56,57,58</sup>. The two existing schemes, DGLAP<sup>59</sup> and BFKL<sup>60</sup>, describe the evolution towards large values of  $Q^2$  and  $1/x_{Bj}$  respectively. Thus for low  $x_{Bj}$  and moderate  $Q^2$  the  $k_t$ -ordered DGLAP evolution should be inappropriate. A solution of the parton evolution equation by CCFM<sup>61</sup> approximates the BFKL equation in the low  $x_{Bj}$  limit and the DGLAP prediction in the high  $x_{Bj}$  limit.

The observation of an increased rate of forward jets was proposed<sup>62</sup> as a signature of BFKL-like parton evolution. This method asks for jets with a high longitudinal momentum fraction  $x_{jet} = p_z/E_{proton}$  (where the parton density functions are well known), for low  $x_{Bj}$  (where the phase space for parton radiation along the gluon ladder is large) and for  $E_{T,jet}^2$  close to  $Q^2$  (which suppresses the DGLAP parton evolution). The ZEUS collaboration<sup>55</sup> finalised their results on forward jet cross-sections. They found an excess at low  $x_{Bj}$  compared to what DGLAP based LO QCD models like HERWIG<sup>34</sup> or LEPTO<sup>63</sup> predict (see Fig. 8). The ARIADNE<sup>64</sup> model, which incorporates one of the main features of the BFKL dynamics, namely the ab-

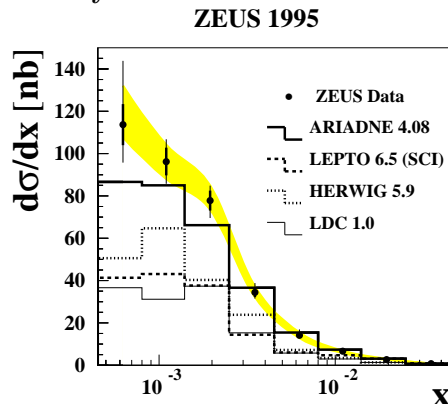


Figure 8: Forward jet cross sections as a function of  $x_{Bj}$ .

sence of the  $k_T$ -ordering in the parton cascade, describes the data reasonably well. Whether this is purely an effect from  $k_T$  non-ordering or due to other effects<sup>65</sup> remains to be investigated in detail. The LO QCD model RAPGAP<sup>66</sup> adding resolved photon contribution to shift the hard subprocess towards the central rapidity region, is also able to describe the forward jet cross-section<sup>49</sup>.

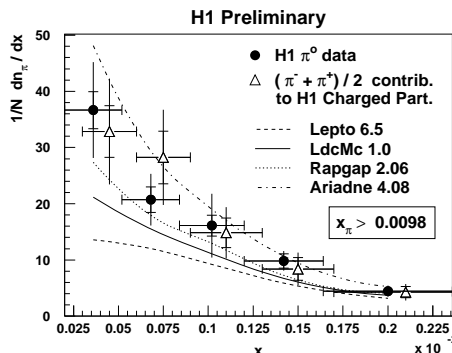


Figure 9: Forward pion rate as function of  $x_{Bj}$ . QCD models are overlaid for comparison.

A complementary approach to gain insights in the parton evolution is to study the production of hard particles in the central rapidity region<sup>68</sup>. Charged or neutral particles at high  $E_T$  are well correlated to parton activity. Their production rate can be directly predicted by analytic calculations folded with proper fragmentation functions<sup>69</sup>. The rate of  $\pi^0$  and  $\pi^\pm$  also exhibits a rise towards small  $x_{Bj}$  (see Fig. 9)<sup>54</sup>.

An important step to improve our understanding of low- $x$  physics is the Linked Dipole Chain (LDC) model<sup>70</sup>. A Monte Carlo implementation of this model<sup>57</sup> was presented for the first time at this workshop.

An analytical BFKL calculation<sup>67</sup> predicts the rise of the cross-section towards small  $x_{Bj}$ , but is higher than the data. These calculations are carried out in LO and the absolute cross-section normalisation is not well known. Moreover, hadronisation corrections can be large, especially at low  $x_{Bj}$  and are very model dependent.

A general disadvantage of these calculations is the lack of a jet algorithm, which has to be applied in the experimental analyses to find the jets. Now new calculations<sup>56,58</sup> have shown that the predicted cross-section can easily change by a factor two when kinematic constraints, like energy-momentum conservation, are applied.

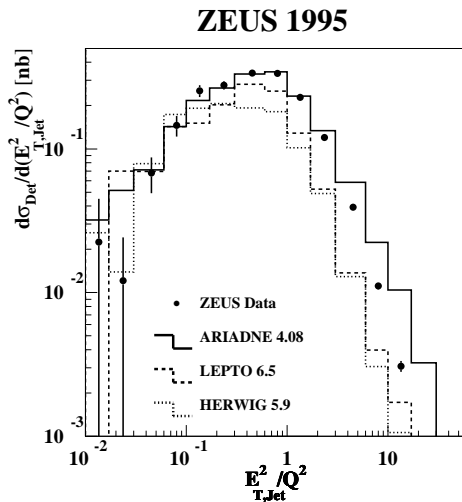


Figure 10: Forward jet cross section (detector level) as a function of  $E_{T,jet}^2/Q^2$ .

It allows to simulate the full hadronisation on top of a CCFM-based parton evolution. Here the trick, which makes the CCFM-type parton evolution in a QCD Monte Carlo applicable, is to move as many as possible initial state branchings to the final state of the shower. However, the prediction of the first released version is below the data. Another approach, even closer to the original CCFM equations, is in progress<sup>56</sup>. Both approaches could eventually result in a Monte Carlo simulation, which successfully describes the full phase space from photoproduction up to very high  $Q^2$ . How well the available QCD models behave in such an extended phase space can be seen<sup>55</sup> in Fig. 10. Here the DIS regime with  $E_{T,jet}^2 \ll Q^2$  is followed by the BFKL-like regime, where  $E_{T,jet}^2 \approx Q^2$ , and finally ends in the region where the hard scale is set by the jet  $E_{T,jet}^2 \gg Q^2$ . While in the DIS regime all QCD models describe reasonably well the data, in the BFKL regime only ARIADNE comes close to the data. In the photoproduction regime all models fail. In conclusion, this field needs much more work, before firm conclusions can be drawn. The driving mechanism behind the parton dynamics especially at low  $x_{Bj}$  is not yet understood.

## 8 High $E_T$ Jet Production in $p\bar{p}$ Collisions

The TEVATRON collider offers the opportunity to investigate the properties of hard interactions in  $p\bar{p}$  collisions at distance scales of approximately  $10^{-17}$  cm. The DØ and CDF collaborations presented analyses of the inclusive jet cross-section, the triple differential dijet cross-section, the dijet mass spectrum, and the dijet angular distribution<sup>71</sup> which were all compared to  $\mathcal{O}(\alpha_s^3)$  QCD predictions.

As previously reported, CDF observed an excess of high  $E_T$  jets with respect to a specific QCD prediction in the inclusive jet cross-section. Both DØ and CDF have released new, preliminary results with the 1994–95 data sets. The CDF result for jets within  $0.1 < |\eta| < 0.7$  is in good agreement with the previous measurement<sup>72</sup> and shows when compared to EKS NLO calculation<sup>73</sup> an excess of events at high  $E_T$ . The JETRAD NLO QCD prediction<sup>74</sup> is, however, in good agreement with the DØ data for the rapidity ranges  $0.1 < \eta < 0.7$  and  $|\eta| < 0.5$  at all values of  $E_T$ . In the range  $|\eta| < 0.5$  the  $\chi^2$  for the data-theory comparison is 23.1 for 24 degrees of freedom. The excess of the high  $E_T$  jets in the inclusive jet cross-section found by CDF was often interpreted as a possible sign for a substructure. Compositeness scales up to 2 TeV are, however, ruled out by an analysis of dijet angular distribution.

Both experiments also measured the ratio of the inclusive jet cross-section at  $\sqrt{s} = 1800$  and 630 GeV as a function of  $x_T = 2E_T/\sqrt{s}$  (as depicted in

Fig. 11). The data are approximately 15% below the NLO QCD predictions.

CDF presented a measurement of the dijet triple differential cross section at  $\sqrt{s} = 1800$  GeV. The data are compared to the JETRAD prediction and show a slight excess of events with high  $E_T$  jets. In addition measurements by both CDF and DØ of the dijet mass spectrum are in good agreement with each other and no significant deviation from theory is seen.

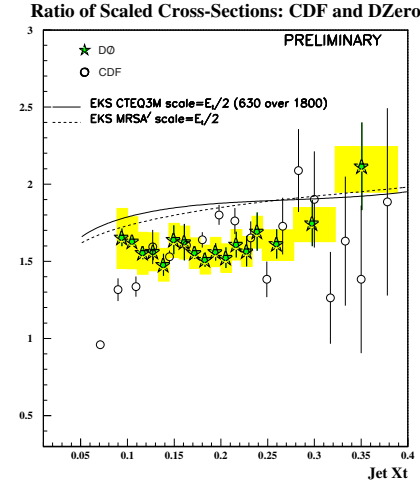


Figure 11: The ratio of the inclusive jet cross sections at  $\sqrt{s} = 1800$  and 630 GeV as a function of  $x_T$ . The shaded regions are the systematic uncertainties of the DØ result.

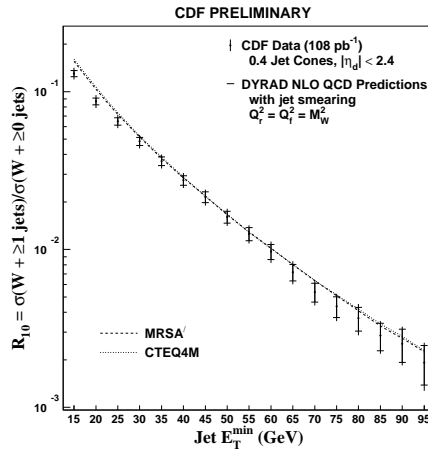


Figure 12: CDF's measurement of  $R_{10} \equiv \sigma(W + \geq 1 \text{ Jet}) / \sigma(W)$  compared to the theoretical prediction.

## 9 $W^\pm$ and $Z^0$ Production in $p\bar{p}$ Collisions

The hadronic interactions of the  $W^\pm$  and  $Z^0$  bosons provide a clean probe of pQCD predictions. Several analyses by DØ and CDF<sup>71</sup> profit from the large sample of  $p\bar{p}$  collisions taken during the 1994-96 collider runs.

At the DIS97 conference DØ presented results<sup>75</sup> which showed an excess of jet production in the exclusive ratio of  $W^\pm + 1$  jet to  $W^\pm + 0$  jet production ( $R_{10}$ ) when compared to the NLO QCD prediction<sup>76</sup>. The CDF collaboration reported on the production cross-section for  $W^\pm + \geq n$  jets. The measured cross-sections are a factor of 1.7 larger than the LO QCD predictions<sup>77</sup>, but are in excellent agreement when compared to DYRAD. This is illustrated in Fig. 12, where  $R_{10}$  as a function of the jet  $E_T$  is shown. The discrepancy between the DØ and CDF results is currently unexplained. The most obvious difference between the two measurements is that DØ uses a cone radius  $R = 0.7$

while CDF uses  $R = 0.4$ . We look forward to the updated DØ results.

From the inclusive production cross-section for both the  $W^\pm$  and  $Z^0$  bosons<sup>71</sup> DØ extracted the total width of the  $W^\pm$ :  $\Gamma = 2.126 \pm 0.092 \text{ GeV}$ . A direct measurement of  $\Gamma$  by CDF using the tail of the transverse mass distribution leads to:  $\Gamma = 2.19_{-0.16}^{+0.17}(\text{stat}) \pm 0.09(\text{syst}) \text{ GeV}$ . Both of these measurements give a consistent picture with other electroweak measurements within the Standard Model.

A measurement of the  $W^\pm$  and  $Z^0$  transverse momentum distributions was made by DØ. In particular the  $p_T^Z$  distribution is able to distinguish between two available models<sup>78,79</sup> for the non-perturbative contributions.

The NuTeV collaboration presented<sup>80</sup> a new indirect measurement of the  $W^\pm$  mass:  $M_{W^\pm} = 80.54 \pm 0.11 \text{ GeV}$ . DØ and CDF presented direct measurements of the  $W^\pm$  mass of:  $M_{W^\pm} = 80.43 \pm 0.11 \text{ GeV}$  (DØ), and  $M_W^\pm = 80.38 \pm 0.12 \text{ GeV}$  (CDF).

### Instanton Induced Events

In QCD anomalous non-perturbative processes are expected which violate classical laws like the conservation of chirality. Instantons<sup>81</sup>, non-perturbative fluctuations of the gluon field inducing hard processes, represent tunneling transitions between topologically inequivalent vacua.

In DIS instanton induced processes are dominantly produced in a quark gluon fusion process<sup>82,83</sup>. The virtuality  $Q'^2$  of the quark  $q'$ , originating from a photon splitting into a  $q\bar{q}$  pair in the instanton background, provides a generic hard scale naturally limiting the instanton size  $\rho$  and makes a quantitative prediction of the cross-section possible<sup>83</sup>. In previous DIS workshops progress on the theoretical understanding and on possible experimental search strategies<sup>84</sup> has been reported. First experimental exclusion limits have been derived<sup>85</sup>. The maximally allowed fraction of instanton induced events is  $\mathcal{O}(1\%)$ .

Recently, further progress on reducing the remaining systematic uncertainties on the cross-section predictions has been achieved<sup>86</sup>. A new 2 loop renormalisation group invariant calculation of the instanton density significantly reduces the residual renormalisation scale dependence of the instanton subprocess cross-section. Moreover, recent lattice calculations allowed to constrain the region of validity of the approximations made when deriving the cross-section expected at HERA. The fiducial kinematic region of  $Q'$  and  $x' = Q'^2/2pq'$ , the Bjorken scaling variable associated with instanton subprocess, is found to be  $Q' \gtrsim 8 \text{ GeV}$  and  $x' \gtrsim 0.35$ . For this region and for  $x_{Bj} > 10^{-3}$  and  $0.1 < y < 0.9$  the instanton production cross-section is found to be  $\sigma = 126 \text{ pb}$ . Such a prediction has, however, not yet reached quantitatively the predictive power of pQCD. Given the large data samples

corresponding to about  $40 \text{ pb}^{-1}$  per experiment already collected at HERA, this sizeable cross-section is large enough to pursue dedicated searches for instanton induced processes. The large cross-section of standard DIS processes necessitates, however, an excellent understanding of perturbative pQCD models in the tails of distributions. The construction of observables based on the characteristic features of the hadronic final state of instanton induced events, which allow for a powerful separation from standard DIS processes, will be the key issue for an experimental discovery.

### Event shapes

Measurements of event shape variables provide information about perturbative and non-perturbative aspects of QCD. They allow to fit analytical expressions to data without referring to a fragmentation model by exploiting their characteristic power behaviour. Event shapes have been extensively studied in  $e^+e^-$  experiments at different center of mass energies<sup>3,87</sup>.

Results from  $e^+e^-$  can be compared to DIS in the current hemisphere of the Breit frame. Thanks to the large kinematic range covered at HERA, the dependence of mean event shape values on a hard scale can be studied in one experiment. Event shapes are defined<sup>h</sup> by<sup>i</sup>:

$$T_Z := \frac{\sum_i p_z}{\sum_i |\vec{p}_i|} \quad B_C := \frac{\sum_i |\vec{p}_{Ti}|}{2 \sum_i |\vec{p}_i|} \quad \rho_C := \frac{M^2}{Q^2} = \frac{(\sum_i p_i)^2}{Q^2} \quad (2)$$

In addition the  $C$  parameter  $C = 3(\lambda_1 \lambda_2 + \lambda_2 \lambda_3 + \lambda_3 \lambda_1)$  derived from the eigenvalues  $\lambda_i$  of the linearized momentum tensor is used in the H1 analysis. This analysis<sup>88,89</sup>, already presented at previous workshops<sup>90</sup>, covers momentum transfers  $Q$  from 7 to 100 GeV. The ZEUS collaboration has presented first results at this conference<sup>91</sup> for  $3.3 \lesssim Q \lesssim 71.5$  GeV. In the H1 data all particles enter the event shape calculation, while ZEUS only selects charged particles. As an example, the  $\langle 1 - T_Z \rangle$  as function of  $Q$  and its differential distribution for different  $\langle Q \rangle$  values are shown in Fig. 13. Despite the different analysis technique, reasonable agreement is found. A spherical (pencil-like) configuration corresponds to  $1 - T_Z = 1/2$  (0). The energy flow along the event shape axis becomes more collimated as  $Q$  increases. Some dependence on  $x_{Bj}$  at constant  $\langle Q \rangle$  is seen.

The mean event shapes can be expressed by a perturbative part calculable in NLO<sup>42,43</sup> and a non-perturbative contribution of the form<sup>92</sup>:

$$\langle F \rangle^{pow} = a_F \frac{16}{3\pi} \frac{\mu_i}{Q} \ln^p \frac{Q}{Q_0} [\bar{\alpha}_0(\mu_i) - \alpha_s(Q) - (b \ln \frac{Q^2}{\mu_i^2} + k + 2b) \alpha_s^2(Q)] \quad (3)$$

<sup>h</sup>In the H1 analysis some more, slightly modified, definitions are studied.

<sup>i</sup>The summation of the four-vector  $p_i = (E_i, \vec{p}_i)$  extends over all objects  $i$  (energy depositions, hadrons or partons) in the current hemisphere of the Breit frame.

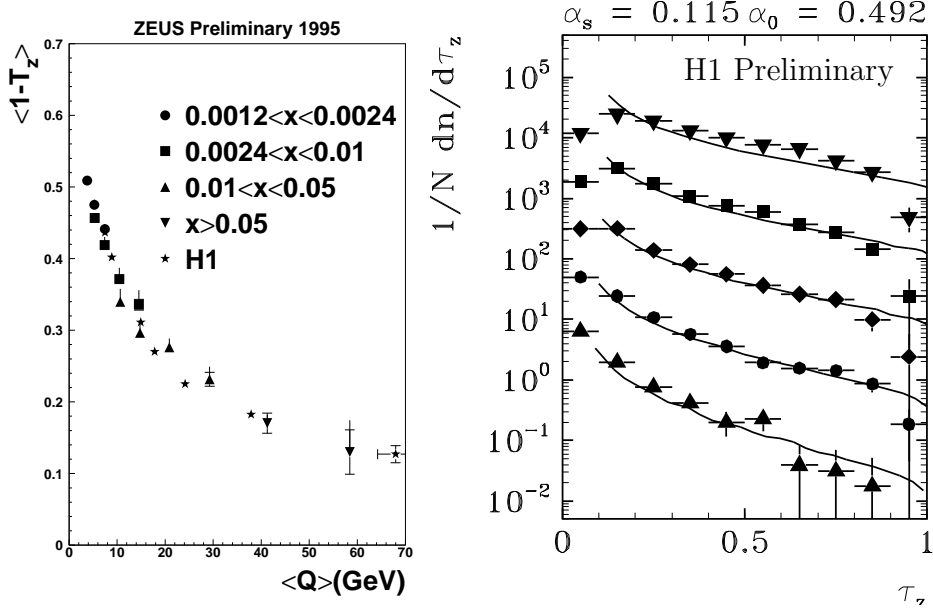


Figure 13: a)  $\langle 1 - T_Z \rangle$  distribution as a function of  $\langle Q \rangle$  from H1 and ZEUS. b) Differential  $\tau_Z = \langle 1 - T_Z \rangle$  distribution for several  $Q$  bins together with the NLO + power correction theory predictions based on the fit parameters obtained from the mean event shapes. The spectra from top to bottom for  $\langle Q \rangle$  values 14.9, 17.8, 24.2, 37.9 and 68 GeV are multiplied by factors of  $10^n$  for  $n = 0, \dots, 4$ .

where  $b = (11 C_A - 2f)/12\pi$  and  $k = [(67 - 3\pi^2) C_A - 10 f]/36\pi$  and  $\bar{\alpha}_0$  is a free, but 'universal', effective coupling parameter below an 'infra-red' matching scale  $\mu_i$ . Some of the calculable coefficients  $a_F$  and  $p$  have recently been reevaluated in the light of non-perturbative two-loop corrections and a common (Milan) factor in eq. 3 has been introduced<sup>93</sup>.  $p$  is only different from 0 for the  $B_C$ . The power corrections are large at low  $Q$ , but become less important with increasing  $Q$ .  $\alpha_s$  and  $\bar{\alpha}_0$  can be simultaneously fitted to the data.

QCD fits show<sup>89</sup> that the analytical form of the power correction is adequate to describe the data. Only for  $B_c$  the theoretically derived additional factor  $\ln Q/Q_0$  in eq. 3 is not supported by the data. The 'universality' of  $\bar{\alpha}_0$  is confirmed when using  $T_Z$  and  $\rho_C$ . The  $B_c$  and the  $C$  parameter give less consistent results. Power corrections to differential distributions have not yet been calculated in DIS. A reasonable description of the data can, however, be obtained by a simple shift of the distribution like expected from calculations



for  $e^+e^-$ . The resulting fit values are however larger than the ones obtained from the mean values. As illustration, the  $1 - T_Z$  is shown in Fig. 13b together with the theory curves predicted from the fit to the mean values.

## Fragmentation Functions and Colour Recombination

Fragmentation functions characterize the complete process of hadron formation including the QCD parton evolution. They are most conveniently studied in the current region of the Breit frame, since there DIS events can be directly compared to  $e^+e^-$  events in one hemisphere. As for the proton structure function, scaling violations are expected. With increasing  $Q^2$ , more phase space is available and consequently more gluons are emitted. To some extent this effect is reduced by the fact that  $\alpha_s$  gets smaller, but the result is a softer particle momentum spectrum.

Therefore more (less) particles are observed at low (large) scaled momenta  $x_p = 2p/Q$  for higher  $Q^2$ . The dependence of  $1/\sigma d\sigma/dx_p$  on  $Q^2$  for various  $x_p$  bins is shown<sup>96</sup> in Fig. 14. At intermediate  $x_p$  approximative scaling is observed. At high  $x_p$  a violation of this scaling is apparent, i.e. less particles with high momentum are found with increasing  $Q^2$ . The decreasing  $1/\sigma d\sigma/dx_p$  at low  $x_p$  and  $Q^2$  is due to mass effects depopulating the current hemisphere induced by boson-gluon fusion processes. The HERA data overlap well within the kinematic range of  $e^+e^-$  data and good agreement between both types of experiments is found. NLO calculations folded with a fragmentation function<sup>95,94</sup> describe the measured distributions well<sup>96</sup> in the region of high  $Q^2, x_p$ , where the theory is applicable. More recent NLO calculations<sup>95,97</sup> allow to vary the QCD parameter  $\Lambda$  and thus will offer the possibility to determine  $\alpha_s$ , when the origin of large fit uncertainties to  $e^+e^-$  data is better understood<sup>96</sup>. Good agreement with the data is found in the high ( $x_p, Q^2$ ) region where the theory is applicable.

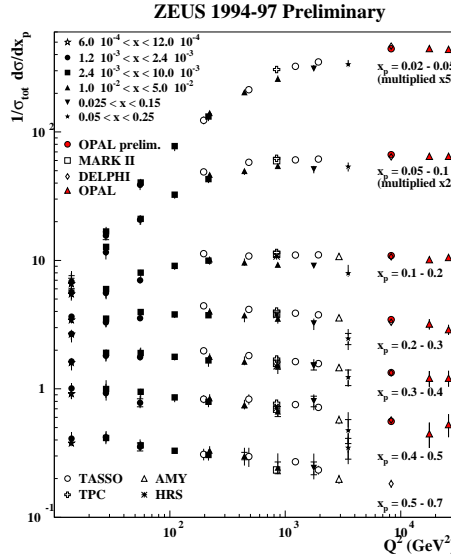


Figure 14: Fragmentation function in  $x_p$  bins vs  $Q^2$ .

Fragmentation functions from individual particle species in jets produced in  $\gamma p$  collisions have been measured at HERA<sup>98</sup>. Their evolution with the scaled energy with respect to the jet energy is tested. Charged hadrons and kaon production are studied separately. The direct component in the photo-production samples behave very similar to the particles in the DIS samples and both are well consistent with results from  $e^+e^-$  experiments (see Fig. 5 in ref.<sup>96</sup>). This supports universality of fragmentation in different reactions, if the appropriate observables are studied.

However, the mechanism driving the transition of partons to hadrons is little understood. In the perturbative regime some colour related effects like soft colour coherence have been successfully calculated, e.g. the modified leading log approximation (MLLA)<sup>99</sup>. Any effect, with which one can study low-energy colour interactions helps to understand the nature of non-perturbative QCD better.  $W$ -pair production at LEP<sup>100</sup> is used to investigate colour re-combinations effects. Events with 4-jets are selected as  $W^\pm$  pair candidates.

If the two proper jets are found, the  $W^\pm$  mass can be reconstructed. Soft colour reconnection could smear out the width of the  $W^\pm$  mass peak. The LEP experiments have searched for this effect, but so far the results do not show a statistically significant signal, see Fig. 15. Similar conclusions are drawn for other observables like multiplicity differences or Bose-Einstein correlation effects. A more sophisticated method<sup>100</sup> tries to reconstruct the colour flow event by event and might be more sensitive to recombination effects.

## Conclusions

The high statistics available in DIS experiments now allows to assess details of the parton fragmentation and of QCD effects. An impressive amount of data is successfully described by NLO calculations. In particular, in jet production in DIS significant progress has been recently made. The transition from non-perturbative to the perturbative regime, and the parton dynamics at low  $x$  have attracted strong interest from experimentalists and from theorists. We are just at the beginning of a global understanding for the various interesting phenomena observed here.

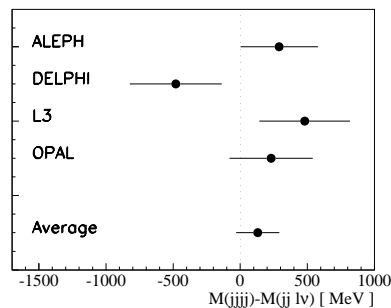


Figure 15: Invariant mass difference in  $W^\pm$  pair production events with 2 and 4 jets.

## Acknowledgments

We would like to thank all speakers of our session for an inspiring working group session and P. Marage and R. Roosen for the excellent organisation of the workshop.

## References

1. in: DIS 96, eds. G. D'Agostini, A. Nigro, Rome 1996.
2. in: DIS 97, eds. J. Repond and D. Krakauer, Chicago 1997.
3. For recent reviews see: S. Bethke, in: QCD 97, Montpellier, Jul. 1997 and PITHA 97/37; S. Bethke, QCD 96, Montpellier, Jul. 1996 and Nucl. Phys. (Proc. Suppl) 54 A (1997) 314 and references therein.
4. R. Bürgin, these proceedings.
5. PLUTO Collab., Phys. Lett. B149 (1984) 421; TPC/2 $\gamma$  Collaboration, H. Aihara et al., Phys. Rev. D41 (1990) 2667; S. E. Baru et al., Z. Phys. C53 (1992) 219.
6. A. Donnachie, P. Landshoff, Phys. Lett. B296 (1992) 227.
7. H1 Collab., Z. Phys. C 69 (1995) 27; ZEUS Collab., Z. Phys. C 63 (1994) 391.
8. CDF Collab., Phys. Rev. D 50 (1994) 5550.
9. G. Schuler, T. Sjöstrand, Z. Phys. C 73 (1997) 677; R. Engel, J. Ranft, Phys. Rev. D 54 (1996) 4244; R. Engel, Z. Phys. C 66 (1995) 203.
10. M. Kienzle, these proceedings.
11. M. Drees et al., Phys. Lett. B 306 (1993) 371.
12. H1 Collab., Z. Phys. C72 (1996) 573.
13. H1 Collab., Phys. Lett. B358 (1995) 412.
14. M. Krücker, these proceedings.
15. S. Frixione et al., Nucl. Phys. B 454 (1995) 3; Phys. Lett. B 348 (1995) 633.
16. B. Kniehl, G. Kramer, M. Spira, Z. Phys. C 76 (1997) 689; J. Binnewies, B. Kniehl, G. Kramer, Z. Phys. C 76 (1997) 677; M. Cacciari et al., Phys. Rev. D 55 (1997) 2736.
17. C. Peterson et al., Phys. Rev. D 27 (1983) 105.
18. N. Zotov, these proceedings.
19. M. Sutton, these proceedings.
20. G. Ingelman, J. Rathsman, G. Schuler, Comp. Phys. Com. 101 (1997) 135.
21. R.K. Ellis, P. Nason, Nucl. Phys. B 312 (1989) 551; J. Smith, W.L. von Neerven, Nucl. Phys. B 374 (1992) 36; S. Frixione et al., Phys. Lett. B 348 (1994) 633.
22. G. Tsipolitis, these proceedings.
23. M. Martinez, these proceedings.
24. ZEUS Collab., DESY-98-038, submitted to Eur. Phys. J. C.
25. OPAL Collab., Z. Phys. C 63 (1994) 197.
26. M. Wobisch, these proceedings.
27. S. Ellis, D. Soper, Phys. Rev. D 48 (1993) 3160.

28. ZEUS Collab., Phys. Lett. B 384 (1996) 401.
29. S. Frixione, G. Ridolfi, Nucl. Phys. B 507 (1997) 315.
30. M. Klasen, G. Kramer, Z. Phys. C72 (1996) 107, idid. C76 (1997) 489.
31. B. W. Harris, J.F. Owens, FSU-HEP-9712256, DESY 97-234.
32. L. Sinclair, these proceedings.
33. T. Sjöstrand, Comp. Phys. Commun. 82 (1994) 74.
34. G. Marchesini et al., Comp. Phys. Comm. 67 (1992) 465.
35. H1 Collab., Phys. Lett. B 346 (1995) 415.
36. ZEUS Collab., Phys. Lett. B 363 (1995) 201.
37. K. Flamm, in: 1.
38. D. Graudenz, Phys. Lett. B256 (1992) 518; Phys. Rev. D49 (1994) 3291; Comp. Phys. Comm. 92 (1995) 65.
39. T. Brodtkorb, J.G. Körner Z. Phys. C 54 (1992) 519; T. Brodtkorb, E. Mirkes, Z. Phys. C 66 (1995) 141.
40. JADE Collab., Z. Phys. C33 (1986) 23.
41. K. Rosenbauer, in: 1.
42. E. Mirkes, D. Zeppenfeld, Phys. Lett. B380 (1996) 205.
43. S. Catani, M. Seymour, Nucl. Phys. B485 (1997) 291.
44. B. Pötter, G. Kramer, Eur. Phys. J. C 1 (1998) 261.
45. G. Graudenz, hep-ph/9710244
46. T. Trefzger, in: 1.
47. N. Tobien, these proceedings.
48. D. Mikunas, M. Weber, M. Wobisch, in: 2.
49. H. Jung, L. Jönsson, H. Küster, DESY-98-051, May 1998.
50. B. Pötter, these proceedings.
51. N. Kidonakis, these proceedings.
52. S. Catani, Y. Dokshitzer, B. Webber, Phys. Lett. B 285 (1992) 291.
53. Y. Dokshitzer, G. Leder, S. Moretti, B.R. Webber, hep-ph/9707323.
54. T. Wengler, these proceedings.
55. M. Riveline, these proceedings; ZEUS Collab., hep-ex/9805016
56. G. Salam, these proceedings.
57. L. Lönnblad, these proceedings.
58. J. Stirling, these proceedings.
59. V.N. Gribov, L.N. Lipatov, Sov. J. Nucl. Phys. 15 (1972) 438 and 675; Y. Dokshitzer, Sov. Phys. JETP 46 (1977) 641; G. Altarelli, G. Parisi, Nucl. Phys. B 126 (1977) 298.
60. E.A. Kuraev, L.N. Lipatov, V.S. Fadin, Sov. Phys. JETP 45 (1977) 199; Y.Y. Balitzki, L.N. Lipatov, Sov. J. Nucl. Phys. 28 (1978) 822.
61. M. Ciafaloni, Nucl. Phys. B 296 (1988) 49; S. Catani, F. Fiorani, G. Marchesini, Phys. Lett. B 234 (1990) 339; Nucl. Phys. B 336 (1990) 18; G. Marchesini, Nucl. Phys. B 445 (1995) 49.
62. A.H. Mueller, Nucl. Phys. B (Proc. Suppl) 18 C (1990) 125; A.H. Mueller, J. of Phys. G 17, (1991) 1443.
63. G. Ingelman, A. Edin, J. Rathsman, Comp. Phys. Comm. 101 (1997) 108.

64. L. Lönnblad, *Comp. Phys. Comm.* 71 (1992) 15.
65. J. Rathsmann, *Phys. Lett. B* 393 (1997) 181.
66. H. Jung, *Comp. Phys. Comm.* 86 (1995) 147.
67. J. Bartels et al., *Phys. Lett. B* 384 (1996) 300.
68. M. Kuhlen, *Phys. Lett. B* 382 (1996) 441.
69. J. Kwieciński, S.C. Lang, A.D. Martin, *Phys. Rev. D* 55 (1997) 1273.
70. B. Andersson, G. Gustafson, J. Samuelsson, *Nucl. Phys. B* 467 (1996) 443; B. Andersson, G. Gustafson, H. Kharraziha, J. Samuelsson, *Z. Phys. C* 71 (1996) 613; B. Andersson, G. Gustafson, H. Kharraziha, *Phys. Rev. D* 57 (1998) 5543.
71. I. Bertram, these proceedings.
72. CDF Collaboration, *Phys. Rev. Lett.* 77 438 (1996).
73. S.D. Ellis, Z. Kunszt, D. Soper, *Phys. Rev. Lett.* 64 (1990) 2121; Z. Kunszt, D. Soper, *Phys. Rev.* 46 (1992) 192.
74. W. T. Giele, E. W. Glover, D.A. Kosower, *Nucl. Phys. B* 403 (1993) 633.
75. T. Joffe-Minor, in: 2.
76. W. T. Giele et al., *Nucl. Phys. B* 403 (1993) 633.
77. F. A. Berends et al., *Nucl. Phys. B* 357 (1991) 32.
78. G. A. Ladinsky, C. P. Yuan, *Phys. Rev. D* 50 (1994) 4239.
79. P. Arnold, R. Kauffman, *Nucl. Phys. B* 349 (1991) 381.
80. J. Yu, these proceedings.
81. A. Belavin et al., *Phys. Lett. B* 59 (1975) 85.
82. I.I. Balitskii, V.M. Braun, *Phys. Lett. B* 346 (1995) 143.
83. S. Moch, A. Ringwald, F. Schrempp, *Nucl. Phys. B* 507 (1997) 134.
84. A. Ringwald, F. Schrempp et al., hep-ph/9411217; hep-ph/9506392 DIS 95; hep-ph/9607238, in: 1; hep-ph/9706399, DIS 97; hep-ph/9706400, in: 2.
85. T. Carli, M. Kuhlen, *Nucl. Phys. B* 511 (1998) 85 and in 3.
86. F. Schrempp, these proceedings.
87. G. Bobbink, these proceedings.
88. H1 Collab., *Phys. Lett. B* 406 (1997) 256.
89. H.-U. Martyn, these proceedings.
90. U. Martyn, K. Rabbertz, in: 1. and 2.
91. R. Waugh, these proceedings.
92. B. Webber, *Phys. Lett. B* 339 (1994) 148; Y. Dokshitzer, B. Webber, *Phys. Lett. B* 352 (1995) 451; M. Dasgupta, B. Webber, *Eur.Phys.J. C* 1 (1998) 539.
93. G. Salam, these proceedings.
94. J. Binnewies et al., *Z. Phys C* 65 (1995) 471 and hep-ph/9707269.
95. D. Graudenz, CERN-TH/96-52.
96. J. Okrasinski, these proceedings and references therein.
97. J. Binnewies et al., hep-ph/9803382.
98. ZEUS Collab., *Eur. Phys. J. C* 2 (1998) 77.
99. Y. Dokshitzer et al., *Basics of pQCD*, ed. J.T. Van, Edition Frontiers, 1991; for a recent review: V. A. Khoze, W. Ochs, *Int. J. Mod. Phys. A* 12 (1997) 2949 and references therein.
100. R. Orava, these proceedings.